

# Dineutron and the three-nucleon continuum observables

H. Witała

*M. Smoluchowski Institute of Physics,  
Jagiellonian University, PL-30059 Kraków, Poland*

W. Glöckle

*Institut für theoretische Physik II, Ruhr-Universität Bochum, D-44780 Bochum, Germany*

(Dated: March 3, 2013)

## Abstract

We investigate how strong a hypothetical  $^1S_0$  bound state of two neutrons would affect different observables in the neutron-deuteron reactions. To that aim we extend our momentum space scheme of solving three-nucleon Faddeev equations to incorporate in addition to the deuteron also the  $^1S_0$  dineutron bound state. We discuss effects induced by dineutron on the angular distribution of the neutron-deuteron elastic scattering and cross sections of the deuteron breakup. A comparison to the available data for neutron-deuteron total cross sections and elastic scattering angular distributions cannot decisively exclude a possibility that the two neutrons can form  $^1S_0$  bound state. However, the strong modifications of a final-state-interaction peak of the neutron-deuteron breakup when changing from negative to positive values of the neutron-neutron scattering length seems to exclude existence of dineutron.

PACS numbers: 21.45.-v, 21.45.Bc, 25.10.+s, 25.40.Dn

## I. INTRODUCTION

Investigation of the neutron-deuteron (nd) elastic scattering and the deuteron breakup reaction [1] revealed a number of discrepancies between data and theoretical predictions based on modern nucleon-nucleon potentials such as AV18 [2], CD Bonn [3], and Nijm1, 2 and 93 [4] or on the nuclear forces derived in the framework of chiral perturbation theory [5]. These potentials describe very accurately all existing nucleon-nucleon (NN) data as expressed by the value of  $\chi^2$  per data point close to  $\approx 1$ . Some of these discrepancies can be explained when in addition to pairwise interactions also three-nucleon forces (3NF's) are included in the 3N Hamiltonian. However, some persistently avoid explanation and they reveal high insensitivity to the underlying dynamics, especially to different choices among available 3NF's. The neutron-neutron (nn) quasi-free-scattering (QFS) configuration in the complete nd breakup is one such an example. Another is the symmetrical space-star (SST) geometry in that reaction. The nn QFS refers to the kinematical configuration in which the outgoing proton is at rest in the laboratory system. In case of SST three outgoing nucleons have equal magnitudes of momenta, which in the three-nucleon c.m. system form a plane perpendicular to the incoming nucleon momentum with the angle of  $120^\circ$  between two consecutive momenta. In QFS and SST configurations theoretical predictions drastically underestimate by about  $\approx 20\%$  the data. This together with the fact that cross sections in these configurations are dominated by the  $^1S_0$  and  $^3S_1$  contributions lead to suspect that something is wrong with the  $^1S_0$  nn force and that maybe two neutrons can even form a bound state [6, 7].

That motivated us to investigate what consequences the existence of the  $^1S_0$  dineutron would have on different observables in nd reactions and to what degree the available data for nd reactions allow for such a bound state. Also we would like to see if existence of dineutron could help in resolving the discrepancies present in QFS and SST nd breakup configurations.

In section II we extend our formulation of the momentum space treatment of the 3N Faddeev equations to include, in addition to the deuteron, also the  $^1S_0$  bound state of two neutrons. Changing the strength of  $^1S_0$  nn interaction of the CD Bonn potential we produce a number of forces which allow for two neutrons being bound with different dineutron binding energy. In section III we present theoretical predictions based on solution of 3N Faddeev equations and compare them to the available nd data. We summarize and conclude in section IV.

## II. FADEEV EQUATIONS WITH DINEUTRON

We shortly present the basics of our momentum space treatment of 3N Faddeev equations and calculations of the transition operators for different reactions in the 3N continuum based on solutions of these equations. For detailed presentation we refer to [1, 8]. We put emphasis on changes in the standard approach in the case when, beside the deuteron, also one additional bound state appears in some partial wave.

For calculation of processes initiated from a state  $|\Phi_{1,1}\rangle \equiv |\vec{q}_0, \phi_d\rangle$ , which describes the neutron moving with the relative momentum  $\vec{q}_0$  with respect to the deuteron of the wave function  $\phi_d$ , one needs the state  $|T\rangle$  which fulfills 3N Faddeev equation

$$|T\rangle = tP|\Phi_{1,1}\rangle + tPG_0|T\rangle, \quad (1)$$

where  $P$  is defined in terms of transposition operators of three nucleons,  $P = P_{12}P_{23} + P_{13}P_{23}$ ,  $G_0$  is the free 3N propagator, and  $t$  is the two-nucleon off-shell t-matrix. Knowing  $|T\rangle$  the breakup as well as the elastic nd scattering amplitudes can be gained by quadratures in the standard manner [1]. Namely, the transition amplitude for the elastic scattering,  $\langle \Phi'_{1,1}|U|\Phi_{1,1}\rangle$ , is given by [1, 8]

$$\langle \Phi'_{1,1}|U|\Phi_{1,1}\rangle = \langle \Phi'_{1,1}|PG_0^{-1}|\Phi_{1,1}\rangle + \langle \Phi'_{1,1}|P|T\rangle, \quad (2)$$

and for the breakup,  $\langle \Phi_0|U_0|\Phi_{1,1}\rangle$ , by

$$\langle \Phi_0|U_0|\Phi_{1,1}\rangle = \langle \Phi_0|(1+P)|T\rangle. \quad (3)$$

The state  $|\Phi_0\rangle \equiv \frac{1}{\sqrt{2}}(1 - P_{23})|\vec{p}\vec{q}\rangle$  corresponds to a kinematically complete configuration of the breakup described by standard Jacobi momenta  $\vec{p}$  and  $\vec{q}$ , and  $|\Phi'_{1,1}\rangle$  is the outgoing state of the elastic scattering with changed direction of the relative neutron-deuteron momentum  $\vec{q}_0'$  but with the same magnitude as in the entrance channel  $|\vec{q}_0'| = |\vec{q}_0|$ .

Introducing the momentum space 3N partial wave basis  $|pq\alpha\rangle \equiv |pq(ls)j(\lambda 1/2)I(jI)J(t 1/2)T\rangle$  with the two-body subsystem angular momenta, spin and isospin  $(ls)j$  and  $t$ , coupled together with the corresponding quantum numbers of the spectator nucleon  $(\lambda 1/2)I$  and  $1/2$  to the total angular momentum  $J$  and isospin  $T$  of the 3N system, and projecting Eq. (1) on these states, we get the system of coupled integral equations in two continuous variables  $p$  and  $q$ . For details of the numerical treatment of that system, and particularly of the kernel part  $\langle pq\alpha|tPG_0|T\rangle$ , we refer to [1].

The 2-nucleon t-matrix conserves the spectator momentum  $q$  and all discrete quantum numbers except the orbital angular momentum  $l$ :

$$\langle pq\alpha|t|p'q'\alpha'\rangle = \frac{\delta(q-q')}{q^2} t_{l_\alpha l_{\bar{\alpha}}}^{s_\alpha j_\alpha t_\alpha}(pp'; E(q) = E - \frac{3}{4m}q^2) \delta_{s_\alpha s_\alpha'} \delta_{j_\alpha j_\alpha'} \delta_{t_\alpha t_\alpha'} \delta_{l_\alpha l_{\bar{\alpha}}'} \delta_{l_{\bar{\alpha}} l_{\bar{\alpha}}'} \delta_{I_\alpha I_{\alpha'}} \quad (4)$$

and has a pole in channels  $\alpha$  for which two-nucleon subsystem has bound state.

In the channels  $|\alpha\rangle = |\alpha_d\rangle$  which contain the 2-body  ${}^3S_1 - {}^3D_1$  states we extract the deuteron pole. Thus we define

$$t_{l_\alpha l_{\bar{\alpha}}}^{s_\alpha j_\alpha t_\alpha}(p, p'; E(q)) \equiv \frac{\hat{t}_{l_\alpha l_{\bar{\alpha}}}^{s_\alpha j_\alpha t_\alpha}(p, p'; E(q))}{E + i\epsilon - \frac{3}{4m}q^2 - \epsilon_d} \quad (5)$$

for the deuteron quantum numbers  $s_\alpha = j_\alpha = 1, t_\alpha = 0, l_\alpha, l_{\bar{\alpha}} = 0, 2$  and keep  $t$  as it is otherwise. That pole property obviously carries over to the  $T$ -amplitude and we define just for the  $|\alpha\rangle = |\alpha_d\rangle$  channels

$$\langle pq\alpha|T\rangle = \frac{\langle pq\alpha|\hat{T}\rangle}{E + i\epsilon - \frac{3}{4m}q^2 - \epsilon_d} \quad (6)$$

Since the energy  $E$  of the 3N system is determined by the incoming neutron energy  $E_{cm}$ :  $E = E_{cm} + \epsilon_d \equiv \frac{3}{4m}q_0^2 + \epsilon_d$ , the deuteron pole occurs at  $q = q_0$ .

When beside the deuteron an additional bound state exists in some 2-nucleon partial wave state one needs to extract in channels  $|\alpha\rangle$  which contain that 2-nucleon state the corresponding pole of the t-matrix by performing the same procedure as for the deuteron. Let us assume that this state is a bound state of two neutrons in the  ${}^1S_0$  state with the wave function  $\phi_{nn}$  and the binding energy  $\epsilon_{nn}$ , and let us denote by  $|\Phi_{1,2}\rangle \equiv |\vec{q}_0, \phi_{nn}\rangle$  the two body channel build on such dineutron, from which or to which different reactions can be initiated.

In the channels  $|\alpha\rangle = |\alpha_{1S_0}\rangle$  which contain the  ${}^1S_0$  dineutron we define

$$t_{l_\alpha l_{\bar{\alpha}}}^{s_\alpha j_\alpha t_\alpha}(p, p'; E(q)) \equiv \frac{\hat{t}_{l_\alpha l_{\bar{\alpha}}}^{s_\alpha j_\alpha t_\alpha}(p, p'; E(q))}{E + i\epsilon - \frac{3}{4m}q^2 - \epsilon_{nn}} = \frac{\hat{t}_{l_\alpha l_{\bar{\alpha}}}^{s_\alpha j_\alpha t_\alpha}(p, p'; E(q))}{\frac{3}{4m}(\vec{q}_0^2 - q^2) + i\epsilon} \quad (7)$$

and the dineutron pole occurs at  $q = \bar{q}_0 = \sqrt{q_0^2 + \frac{4m}{3}(\epsilon_d - \epsilon_{nn})}$ . Again that pole property carries over to the  $T$ -amplitude and we define for the  $|\alpha\rangle = |\alpha_{1S_0}\rangle$  channels the amplitude  $\langle pq\alpha|\hat{T}\rangle$  similarly to Eq. (6). The numerical treatment of that new pole follows the treatment of the deuteron pole [1] and it requires the set of q-points which, in addition to  $q = q_0$  needed for numerical treatment of the deuteron pole, contains also  $q = \bar{q}_0$  point. Since the dineutron occurs in the neutron-neutron  ${}^1S_0$  state it implies charge independence breaking and the resulting difference

between  $^1S_0$  nn and np interactions causes that the proper treatment of the nd reactions requires inclusion of the total 3N system isospin component  $T = 3/2$  for channels  $\alpha$  containing  $^1S_0$  [9].

The existence of  $^1S_0$  dineutron increases number of possible reactions with three nucleons what in consequence makes that the unitary relation have to be generalized to include those additional processes. It has the form

$$\begin{aligned}
& \langle \Phi_{1,a} | U | \Phi_{1,a'} \rangle^* - \langle \Phi_{1,a'} | U | \Phi_{1,a} \rangle \\
&= 2\pi i \sum_{b=1,2} \int d^3q \langle \Phi_{\vec{q},b} | U | \Phi_{1,a'} \rangle^* \delta(E_{\vec{q}}^b - E_{\vec{q}}) \langle \Phi_{\vec{q},b} | U | \Phi_{1,a} \rangle \\
&+ 2\pi i/6 \int d^3p d^3q \langle \Phi_0 | U_0 | \Phi_{1,a'} \rangle^* \delta(E_{pq} - E_{\vec{q}}) \langle \Phi_0 | U_0 | \Phi_{1,a} \rangle
\end{aligned} \tag{8}$$

with  $a = 1$  and  $2$  for the deuteron and dineutron channels, respectively. One can choose  $a' = 1$  or  $a' = 2$  and  $a = 1$  or  $a = 2$ . For  $a = a' = 1$  this leads on the left side to the forward scattering amplitude and on the right to the total cross section. The energies  $E_{\vec{q}}^b = E_{\vec{q}} + E_b$  are given by the binding energies of the deuteron  $E_1 = \epsilon_d$  or dineutron  $E_2 = \epsilon_{nn}$ .

The angular distribution for the process  $n + d \rightarrow p + \text{dineutron}$  is given by the transition amplitude  $\langle \Phi_{1,2} | U | \Phi_{1,1} \rangle$

$$\frac{d\sigma}{d\Omega}(n + d \rightarrow p + \text{dineutron}) = \left(\frac{2m}{3}\right)^2 (2\pi)^4 \frac{\bar{q}_0}{q_0} \sum_{m_p m_n m_d} |\langle \Phi_{1,2} | U | \Phi_{1,1} \rangle|^2, \tag{9}$$

where  $PG_0^{-1}$  and  $PT$  contributions to  $U$  are given by

$$\begin{aligned}
\langle \Phi_{1,2} | PG_0^{-1} | \Phi_{1,1} \rangle &= \langle \phi_{nn}, m_p, \vec{q}_0 | PG_0^{-1} | \phi_d, m_n, m_d, \vec{q}_0 | | \hat{z} \rangle \\
&= \frac{2}{\sqrt{4\pi}} [\epsilon_d - \frac{1}{m} (\frac{1}{4} q_0^2 + \vec{q}_0^2 + \vec{q}_0 \cdot \vec{q}_0)] (\frac{1}{2} \frac{1}{2} 1 | - \frac{1}{2}, -\frac{1}{2}, -1) (\frac{1}{2} \frac{1}{2} 0 | - \frac{1}{2}, \frac{1}{2}, 0) \\
&\quad \phi_{nn}(|\vec{q}_0 + \frac{1}{2} \vec{q}_0|) \sum_{l=0,2} (l11 | m_d + m_n - m_p, -m_n + m_p, m_d) \\
&\quad (\frac{1}{2} \frac{1}{2} 1 | - m_n, m_p, -m_n + m_p) (\frac{1}{2} \frac{1}{2} 0 | m_n, -m_n, 0) \\
&\quad \phi_l^d(|\frac{1}{2} \vec{q}_0 + \vec{q}_0|) Y_{l, m_d + m_n - m_p}(\frac{1}{2} \vec{q}_0 + \vec{q}_0)
\end{aligned} \tag{10}$$

and

$$\begin{aligned}
\langle \Phi_{1,2} | P | T \rangle &= \langle \phi_{nn}, m_p, \vec{q}_0 | P | T \rangle \\
&= \sum_{J^\pi M} \sum_{\alpha' \alpha_0} \delta_{I_0 J} \delta_{l_0 0} \delta_{s_0 0} \delta_{j_0 0} (\lambda_0 \frac{1}{2} I | M - \mu', \mu', M) (1 \frac{1}{2} T_0 | -1, \frac{1}{2}, -\frac{1}{2}) Y_{\lambda_0, M - \mu'}(\hat{\vec{q}}_0) \\
&\quad \int_0^\infty q'^2 dq' \int_{-1}^1 dx \phi_{nn}(\pi_1) \frac{G_{\alpha_0, \alpha'}(\vec{q}_0, q', x)}{\pi_1^{l_0} \pi_2^{l_{\alpha'}}} \langle \pi_2, q', \alpha' | T \rangle,
\end{aligned} \tag{11}$$

with

$$\pi_1 = \sqrt{q'^2 + \frac{1}{4} \vec{q}_0^2 + q' \vec{q}_0 x},$$

$$\pi_2 = \sqrt{\vec{q}_0^2 + \frac{1}{4}q'^2 + q'\vec{q}_0x} . \quad (12)$$

It was assumed that the relative neutron-deuteron momentum  $\vec{q}_0$  in the incoming channel is directed along the z-axis. The convention for isospin projections is that for the neutron it is  $-\frac{1}{2}$  while for the proton  $+\frac{1}{2}$ . In Eq. (11) channels  $\alpha_0$  contain the dineutron two-nucleon subsystem quantum numbers with isospin  $t_0 = 1$  and its projection  $\nu_{t_0} = -1$  and the total isospin  $T_0$  of the 3N system for these channels is  $T_0 = \frac{1}{2}$  or  $T_0 = \frac{3}{2}$ . The geometrical coefficient  $G_{\alpha_0, \alpha'}(\vec{q}_0, q', x)$  stems from the matrix elements of the permutation operator  $P$  [1].

### III. RESULTS

In the following we will present and compare to the available nd data the theoretical predictions for cross sections in elastic nd scattering and breakup assuming different  $^1S_0$  nn force. We take the CD Bonn [3] potential as the NN interaction and multiplying its  $^1S_0$  nn component by a factor  $\lambda$  generate a number of  $^1S_0$  nn forces among which some provide binding of two neutrons. In Table I we show values of the nn scattering length  $a_{nn}$ , the effective range parameter  $r_{eff}$  and the dineutron binding energy  $\epsilon_{nn}$  for a number of  $\lambda$  values. Changing  $\lambda$  from 0.9 to 1.5 leads to nn  $^1S_0$  force with different, negative as well as positive, values of the scattering length. In order to see if conclusions depend from a particular  $^1S_0$  nn potential used and from the method applied to generate the nn bound state, we performed also calculations with a chiral NN potential in next-to-leading-order (NLO) of chiral expansion [5] adjusting its  $^1S_0$  nn low energy constants to get a dineutron with given binding energy.

#### A. Total cross sections

The results for the nd total cross sections are shown in Fig. 1 and, for a number of energies, they are also presented in Table II. The theoretical predictions obtained with different nn  $^1S_0$  forces are compared to numerous data taken over many years. Up to  $\approx 100$  MeV there is a nice agreement between all data, especially very precise one of Ref. [10], and theory based on the CD Bonn potential. When instead of the original CD Bonn  $^1S_0$  nn force the modified interaction with factor  $\lambda = 0.9$  is taken the resulting cross sections seem to be not excluded by the total cross section data. For  $\lambda = 1.21$ , with the dineutron binding energy  $\epsilon_{nn} = -144$  keV, the predicted total cross sections for energies up to  $\approx 10$  MeV differ from the data by about three standard deviations.

At higher energies they clearly lie outside three standard deviations from the data. Increasing the factor  $\lambda$  to 1.3 or 1.4 leads to total cross section values strongly overestimating the data.

In Figs. 2 and 3 we compare theoretical predictions for the total elastic scattering and breakup cross sections, respectively, with the corresponding data. For the elastic scattering component of the total cross section (see Fig. 2), at energies up to about  $E_n \approx 20$  MeV, the theoretical predictions with different nn  $^1S_0$  forces are close to each other and they agree with the data. At energies above  $E_n \approx 20$  MeV cross sections for  $\lambda > 1$  start to deviate from standard CD Bonn and  $\lambda = 0.9$  values and the data seems to prefer larger values of  $\lambda$ .

For the total breakup cross sections (see Fig. 3) the data seems to be compatible with all theoretical predictions with exception of data from Ref. [15]. That data set taken in the region of energies  $12 \text{ MeV} < E_n < 22 \text{ MeV}$  clearly advocates the CD Bonn potential predictions. However, it does not exclude definitely values of cross sections obtained with  $\lambda = 1.21$ .

At low energies the nd interaction is parametrized by the doublet,  $^2a_{nd}$ , and quartet,  $^4a_{nd}$ , scattering lengths. While  $^2a_{nd}$  is strongly influenced by a 3NF the  $^4a_{nd}$  is practically insensitive to such an interaction [16]. In Table III we show how these scattering lengths change with modification of the  $^1S_0$  nn CD Bonn potential. While the doublet scattering length drastically changes with  $\lambda$  the quartet scattering length practically remains constant under such modifications of the  $^1S_0$  nn force staying close to the experimental value  $^4a_{nd} = (6.35 \pm 0.02) \text{ fm}$  [17].

## B. Elastic neutron-deuteron scattering

The nd elastic scattering angular distributions are shown in Fig. 4. At c.m. scattering angles  $\Theta_{c.m.} > 45^\circ$  different theories practically overlap and agree with the data for all four energies shown. Such behaviour is not surprising since at backward angles the exchange term  $PG_0^{-1}$ , given by the deuteron wave function, dominates the elastic scattering transition amplitude. The properties of the nn  $^1S_0$  interaction should play decisive role at forward angles. Indeed, at forward angles below  $\Theta_{c.m.} < 45^\circ$  differences between theoretical predictions based on different nn  $^1S_0$  forces start to appear and they increase with decreasing angle. However, in the forward angular region the nd elastic scattering cross section data are lacking with exception of  $E_n = 14.1 \text{ MeV}$  where 5 data points fall into that region of angles. While two data points at smallest angles support the CD Bonn cross sections three other at greater angles prefer the larger values of  $\lambda$ . The precise nd elastic scattering data at forward angles are required to decide if stronger nn  $^1S_0$  force is allowed.

### C. Breakup

Among numerous kinematically complete breakup configurations the largest discrepancies between theory and data have been found for the nn QFS and SST geometries. For these configurations the theoretical cross sections are insensitive to the underlying dynamics and they do not change when applying different realistic NN potentials and combining them with available 3NF's. Also when instead of the nn QFS one compares the theory with the only one available np QFS data set of the nd breakup [22] a nice agreement is found. QFS and SST configurations are dominated at low energies by the  $^1S_0$  and  $^3S_1$  NN force components [6] which practically saturate the QFS and SST cross section at low energies [6, 7]. It would suggest that it is the nn  $^1S_0$  force which is probably responsible for large discrepancy between data and theory.

For QFS configurations we show in Fig. 5 the sensitivity of the nn and np QFS configurations to the underlying nn  $^1S_0$  force. As expected, changes of that force cause drastic modifications of the nn QFS cross section leaving the np QFS practically without modifications. As was shown in [7] responsible for such drastic modifications of the nn QFS cross section are changes of the effective range parameter induced by factor  $\lambda$ . The changes in the nn scattering length practically leave the nn QFS cross sections without modifications.

In contrast to the nn QFS the SST geometry is more stable against changes of the  $^1S_0$  nn force. As shown in Fig. 6 changing the factor  $\lambda$  does not bring theory closer to the data. While  $\lambda = 0.9$  provides smaller SST cross sections than the CD Bonn potential, taking factor  $\lambda > 1$  and increasing it so that dineutron is formed, leads to cross sections which again are below the CD Bonn potential predictions. Therefore by modifications of the  $^1S_0$  nn force it is not possible to explain the large discrepancy for SST. Since it is improbable that the deuteron properties are so badly known that the  $^3S_1 - ^3D_1$  NN force component would require modification, the source for that disagreement must be sought elsewhere. One possibility could be the indirect influence by the dineutron some breakup configurations by contributing in specific regions of a phase-space to the breakup background.

For the  $^1S_0$  nn force which allows a dineutron the nn scattering length becomes positive. It should have drastic influence on the nn final-state-interaction (FSI) of the nd breakup, where the two outgoing neutrons, having the same momenta, are strongly interacting in the  $^1S_0$  state. We show in Fig. 7 the changes in the FSI peak when the nn scattering length  $a_{nn}$  changes from negative to positive values. For the same magnitude of  $a_{nn}$  the nn FSI cross section is strongly diminished for the positive sign of  $a_{nn}$ . The question arises if the existing nn FSI cross section data can be



understood when dineutron exists ?

To answer that question we show in Fig. 8 cross sections for 4 kinematically complete nn FSI configurations for which data have been taken and analyzed in Ref. [26] with the aim to extract the neutron-neutron scattering length. The consistent values of  $a_{nn}$  have been found in each of those 4 configurations with the average value of  $a_{nn} = 18.7 \pm 0.7$  fm. As can be seen in Fig. 8, again changing  $a_{nn}$  to positive values diminishes significantly the nn FSI cross sections. Comparing cross sections obtained with  $\lambda = 1.19$  and  $\lambda = 1.21$  to the CD Bonn potential values clearly demonstrates that no theoretical analysis of [26] data, when performed with positive values of  $a_{nn}$ , would provide consistent values for the nn scattering length in those 4 geometries. While the analysis of  $\theta_1 = \theta_2 = 43^\circ$  configuration would probably provide  $a_{nn} = +21.69$  fm, a similar analysis of configurations at smaller  $\theta_1 = \theta_2$  would provide distinctly larger positive nn scattering lengths.

In Fig. 9 we show further 3 FSI configurations for which data have been taken. For  $d(n, nn)p$  complete breakup the data of Ref. [24] support the CD Bonn potential cross section predictions. Each of 2 complete configurations in that reaction shown in Fig. 9 contain two np FSI peaks. The theoretical analysis of these np FSI peaks, if performed with positive values of  $a_{nn}$ , would provide different values for the neutron-proton scattering length  $a_{np}$ , which in addition would be inconsistent with well known  $a_{np}$  experimental value.

In Fig. 9 we show also the configuration for  $d(n, np)n$  breakup in which data have been taken and analyzed in Ref. [27]. That geometry contains both np and nn FSI peaks. Again, the analysis of the np FSI peak, if performed with positive  $a_{nn}$ , would provide too large magnitude for  $a_{np}$ .

To see how our conclusions depend on the NN potential used and on the method applied to modify the  $^1S_0$  nn force we present in Fig. 8 also cross sections obtained with next-to-leading-order (NLO) chiral perturbation theory potential of Ref. [5], including in calculations all np and nn forces up to the total angular momentum  $j_{max} = 3$  in the two-nucleon subsystem. The  $^1S_0$  component of that interaction is composed of the one- and two-pion exchange terms and contact interactions parametrized by two parameters  $\tilde{C}_{1S_0}$  and  $C_{1S_0}$

$$V(^1S_0) = \tilde{C}_{1S_0} + C_{1S_0}(p^2 + p'^2) . \quad (13)$$

Standard values are  $\tilde{C}_{1S_0} = -0.1557374 \times 10^4$  GeV<sup>2</sup> and  $C_{1S_0} = 1.5075220 \times 10^4$  GeV<sup>4</sup> for cutoff combinations  $\{\Lambda, \tilde{\Lambda}\} = \{450 \text{ MeV}, 500 \text{ MeV}\}$  [5]. By multiplying  $\tilde{C}_{1S_0}$  by a factor  $C_2(^1S_0)$  and  $C_{1S_0}$  by a factor  $C_1(^1S_0)$ , one can induce changes of the nn  $^1S_0$  interaction. In Fig. 8 we show two predictions based on the NLO potential with negative ( $a_{nn} = -17.6$  fm - the (magenta) dashed-dotted line) and positive ( $a_{nn} = +17.5$  fm - the (green) double-dashed-dotted line) values of the

neutron-neutron scattering length. Comparing them with different CD Bonn potential predictions and taking into account differences between their  $a_{nn}$  values it is clearly seen that both potentials and methods of changing  $^1S_0$  nn interaction lead to the same conclusions.

FSI region can also be investigated in the uncomplete breakup measurement, in which spectrum of the outgoing proton is measured at given lab. angle. In Fig. 10 we show modifications of the outgoing proton spectrum for 14 MeV nd breakup at proton lab. angle  $\theta = 4^\circ$ . Here changing the sign of  $a_{nn}$  leads to disappearing of the FSI peak. In addition, at lower energies of the outgoing proton the modification of  $^1S_0$  nn force by factors  $\lambda > 1$  significantly increases the uncomplete breakup cross section.

The analysis of existing nd uncomplete breakup spectra performed in [28, 29] indicated on the inconsistencies in the experimental uncomplete nd breakup data and revealed unexplained differences of more than 25% in regions of the outgoing proton energies where large number of different three-nucleon configurations contribute to the cross section. The question arises if existence of the dineutron and corresponding modification of the  $^1S_0$  nn force can account for that and if the clear FSI peaks appearing in the experimental outgoing proton spectra provide evidence for existence of dineutron. In order to answer that question a theoretical Monte Carlo analysis of experimental spectra, which would provide the angular distribution for the dineutron cross section, is required. The resulting angular distribution should then be compared to the theoretical angular distribution for  $n + d \rightarrow p + \text{dineutron}$  transition. However, in view of the results presented above for the complete nn FSI configurations for which data are available, it seems highly improbable that analysis of incomplete spectra will provide a clear signal for existence of dineutron.

#### D. Transition from the neutron-deuteron to the proton-dineutron channel

For values of factor  $\lambda = 1.21, 1.3$  and  $1.4$ , which allow for the bound  $^1S_0$  state of two neutrons, the transition to the proton-dineutron channel is possible. In Fig. 11 we show angular distributions for  $n+d \rightarrow p+\text{dineutron}$  reaction. The cross sections for that reaction are by an order of magnitude smaller than for the nd elastic scattering, with largest cross sections at backward c.m. angles for low incoming neutron energies.

In view of the discrepancies found in the nd breakup reaction, especially in SST configuration, it is interesting to consider in which phase-space region that hypothetical dineutron state could mostly affect the breakup configurations by contributing in an uncontrolled manner to the background. To answer that question again Monte Carlo simulations of experimental conditions are required.

#### IV. SUMMARY AND CONCLUSIONS

We have investigated how far available nd data allow for hypothetical  $^1S_0$  bound state of two neutrons and if such dineutron can help to explain the discrepancies between theory and data found in some complete nd breakup configurations. To this aim we extended our numerical momentum space treatment of 3N Faddeev equations to include in addition to the deuteron also  $^1S_0$  dineutron. Solution of these equations with modified nn  $^1S_0$  CD Bonn force provided predictions for cross section in different nd reactions.

We found that available nd data for the total nd interaction cross section are incompatible with the existence of a dineutron with binding energy of absolute value greater than  $\approx 100$  keV. The data for the total elastic scattering and breakup cross sections do not exclude such a possibility. Also data for the nd elastic scattering angular distribution cannot decisively exclude such a state. However, in this case the precise data taken at forward angles, if available, could provide more constraints on existence of a dineutron.

The modifications of the  $^1S_0$  nn force component cannot provide explanation for the drastic discrepancy between theory and data for the SST geometry of the nd breakup. Allowing for dineutron provides even smaller SST cross sections, increasing thus that discrepancy.

The transition from negative to positive nn scattering lengths leads to drastic modifications of the FSI cross sections. In the outgoing proton spectra of the uncomplete nd breakup the positive scattering length leads to strong diminishing of the FSI peak at maximal proton energies. The careful Monte Carlo theoretical analysis of existing proton spectra is required to get answer if these spectra provide a clear signal for the existence of dineutron. However, complete FSI configurations for which data have been taken exclude positive values for  $a_{nn}$ .

#### Acknowledgments

This work was supported by the Polish National Science Center under Grant No. DEC-2011/01/B/ST2/00578. It was also partially supported by the European Community-Research Infrastructure Integrating Activity “Exciting Physics Of Strong Interactions” (acronym WP4 EPOS) under the Seventh Framework Programme of EU. The numerical calculations have been performed

on the supercomputer cluster of the JSC, Jülich, Germany.

---

- [1] W. Glöckle, H. Witała, D. Hüber, H. Kamada, J. Golak, Phys. Rep. **274**, 107 (1996).
- [2] R. B. Wiringa, V.G.J. Stoks, R. Schiavilla, Phys. Rev. C **51**, 38 (1995).
- [3] R. Machleidt, F. Sammarruca, and Y. Song, Phys. Rev. C **53**, R1483 (1996).
- [4] V.G.J. Stoks *et al.*, Phys. Rev. C **49**, 2950 (1994).
- [5] E. Epelbaum, Prog. Part. Nucl. Phys. **57**, 654 (2006).
- [6] H. Witała and W. Glöckle, J. Phys. G: Nucl. Part. Phys. **37**, 064003 (2010).
- [7] H. Witała and W. Glöckle, Phys. Rev. C **83**, 034004 (2011).
- [8] W. Glöckle, The Quantum Mechanical Few-Body Problem, Springer Verlag 1983.
- [9] H. Witała, W. Glöckle, H.Kamada, Phys. Rev. C **43**, 1619 (1991).
- [10] W. Abfalterer *et al.*, Phys. Rev. Lett. **81**, 57 (1998).
- [11] P. Schwarz *et al.*, Nucl. Phys. **A398**, 1 (1983).
- [12] J.D. Seagrave, Phys. Rev. **97**, 757 (1955).
- [13] H.C. Catron *et al.*, Phys. Rev. **123**, 218 (1961).
- [14] M. Holmberg, Nucl. Phys. **A129**, 327 (1969).
- [15] G. Pauletta and F.D. Brooks, Nucl. Phys. **A255**, 267 (1975).
- [16] H. Witała *et al.*, Phys. Rev. C **68**, 034002 (2003).
- [17] W. Dilg, L. Koester, and W. Nistler, Phys. Lett. **36B**, 208 (1971).
- [18] C.R. Howell *et al.*, Few-Body Syst. **16**, 127 (1994).
- [19] J.C. Allred, A.H. Armstrong, and L. Rosen, Phys. Rev. **91**, 90 (1953).
- [20] A.C. Berick, R.A.J. Riddle, and C.M. York, Phys. Rev. **174**, 1105 (1968).
- [21] H. Rühl *et al.*, Nucl. Phys. **A524**, 377 (1991).
- [22] A. Siepe *et al.*, Phys. Rev. C **65**, 034010 (2002).
- [23] H.R. Setze *et al.*, Phys. Lett. **B388**, 229 (1996).
- [24] H.R. Setze *et al.*, Phys. Rev. C **71**, 034006 (2005).
- [25] J. Strate *et al.*, Nucl. Phys. **A501**, 51 (1989).
- [26] D. E. Gonzalez Trotter *et al.*, Phys. Rev. C **73**, 034001 (2006).
- [27] V. Huhn *et al.*, Phys. Rev. C **63**, 014003 (2000).
- [28] W. Tornow, H. Witała, and R.T. Braun, Few-Body Syst. **21**, 97 (1996).
- [29] W. Tornow, R.T. Braun,, H. Witała, N. Koori, Phys. Rev. C **54**, 42 (1996).
- [30] J.M. Clement, P. Stoler, C.A. Gouling, R.W. Fairchild , Nucl. Phys. **A183**, 51 (1972).
- [31] J.D. Seagrave, R.L. Henkel, Phys. Rev. **98**, 666 (1955).
- [32] J.C. Davis, H.H. Batschall, Phys. Rev. C **3**, 1798 (1971).
- [33] C.F. Cook, T.T. Bonner, Phys. Rev. **94**, 651 (1954).

- [34] H.L. Poss, E.O. Salant, G.A. Snow, L.C.L. Yuan, Phys. Rev. **87**, 11 (1952).
- [35] N. Koori, Journ. of the Phys. Soc. of Japan, **32**, 306 (1972).
- [36] S. Shirato, N. Koori, Nucl. Phys. **A120**, 387 (1968).
- [37] D.I. Meyer, W. Nyer, Report LA-1279, 5107.
- [38] R.A.J. Riddle, A. Langsford, P.H. Bowen, G.C. Cox, Nucl. Phys. **61**, 457 (1965).

TABLE I: The dineutron binding energy  $\epsilon_{nn}$ , the nn scattering length  $a_{nn}$  and the effective range parameter  $r_{eff}$  for different factors  $\lambda$  by which the nn  $^1S_0$  component of the CD Bonn potential was multiplied.

$\lambda$	$\epsilon_{nn}$ [MeV]	$a_{nn}$ [fm]	$r_{eff}$ [fm]
0.9	-	-8.25	3.12
1.0	-	-18.80	2.82
1.19	-0.099	+21.69	2.39
1.21	-0.144	+18.22	2.35
1.3	-0.441	+10.95	2.20
1.4	-0.939	+7.87	2.07

TABLE II: The theoretical (evaluated at the nucleon laboratory energy  $E_{th}$ ) and experimental (taken at  $E_{exp}$ ) nd total cross sections. Theoretical values were obtained with the CD Bonn potential the  $^1S_0$  nn component of which was multiplied by a factor  $\lambda$ .

$E_{th}$ [MeV]	$\sigma_{exp}$ [mb]	$E_{exp}$ [MeV]	$\sigma_{th}^{\lambda=0.9}$ [mb]	$\sigma_{th}^{\lambda=1.0}$ [mb]	$\sigma_{th}^{\lambda=1.21}$ [mb]	$\sigma_{th}^{\lambda=1.3}$ [mb]	$\sigma_{th}^{\lambda=1.4}$ [mb]
8.0	$1207 \pm 13$	8.0 [32]	1203.4	1205.6	1258.5	1301.4	1353.5
	$1213.3 \pm 5.58$	8.038 [30]					
	$1224 \pm 10$	8.0 [11]					
10.0	$1055 \pm 10$	10.0 [32]	1026.4	1036.1	1089.9	1123.7	1162.5
	$1051.1 \pm 6.9$	10.026 [30]					
	$1045.0 \pm 3.4127$	9.9218 [10]					
13.0	$867 \pm 12$	12.995 [32]	837.96	851.76	900.91	926.56	954.72
14.1	$803 \pm 14$	14.1 [34]	783.94	798.25	845.37	868.91	894.52
	$790 \pm 20$	14.1 [33]					
	$809 \pm 6$	14.1 [35]					
	$778 \pm 22$	14.1 [36]					
	$806 \pm 6$	14.1 [36]					
	$810 \pm 30$	14.2 [37]					
19.0	$627.96 \pm 12.16$	18.932 [30]	603.47	617.55	655.92	673.20	691.76
	$632 \pm 14$	19.01 [31]					
26.0	$455 \pm 12$	26.015 [32]	444.41	456.18	485.43	497.83	511.16
	$451.47 \pm 17.72$	26.082 [30]					
42.5	$267.7 \pm 3.9$	42.5 [38]	259.24	266.35	283.32	290.27	297.88
65.0	$166.5 \pm 2.9$	63.5 [38]	157.24	160.95	170.27	173.96	178.13
	$161.7 \pm 2.8$	66.5 [38]					
	$168.27.0 \pm 0.48333$	65.039 [10]					

TABLE III: The doublet  $^2a_{nd}$  and quartet  $^4a_{nd}$  nd scattering lengths for different factors  $\lambda$  by which the nn  $^1S_0$  component of the CD Bonn potential was multiplied. The calculations have been done with all partial waves with 2N total angular momenta up to  $j_{max} = 3$  included.

$\lambda$	$^2a_{nd}$ [fm]	$^4a_{nd}$ [fm]
0.9	1.51485	6.34602
1.0	0.93174	6.34600
1.21	-0.43567	6.34596
1.3	-1.18887	6.34593
1.4	-2.37605	6.34589



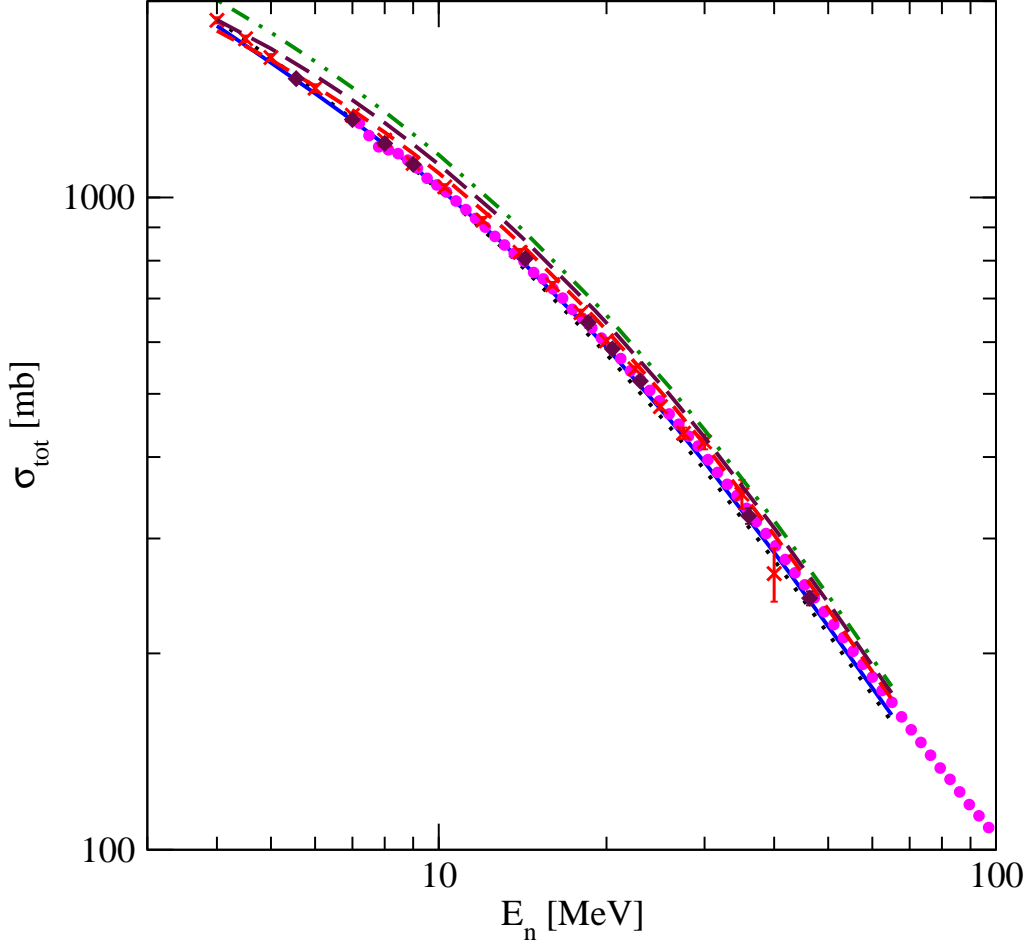


FIG. 1: (color online) The total cross section for the neutron-deuteron interaction as a function of the neutron lab. energy. Different lines show sensitivity of the total cross section to the changes of the nn  $^1S_0$  force component. Those changes were induced by multiplying the  $^1S_0$  nn matrix element of the CD Bonn potential by a factor  $\lambda$ . The solid (blue) line is the full result based on the original CD Bonn potential ( $\lambda = 1.0$ ) and all partial waves with 2N total angular momenta up to  $j_{max} = 3$  included. The (black) dotted, (red) short-dashed, (maroon) long-dashed, and (green) dashed-double-dotted lines correspond to  $\lambda = 0.9$ , 1.21, 1.3, and 1.4, respectively. The (magenta) circles, (red) x-es, and (maroon) diamonds are nd data of Ref. [10], [11], and [12], respectively.

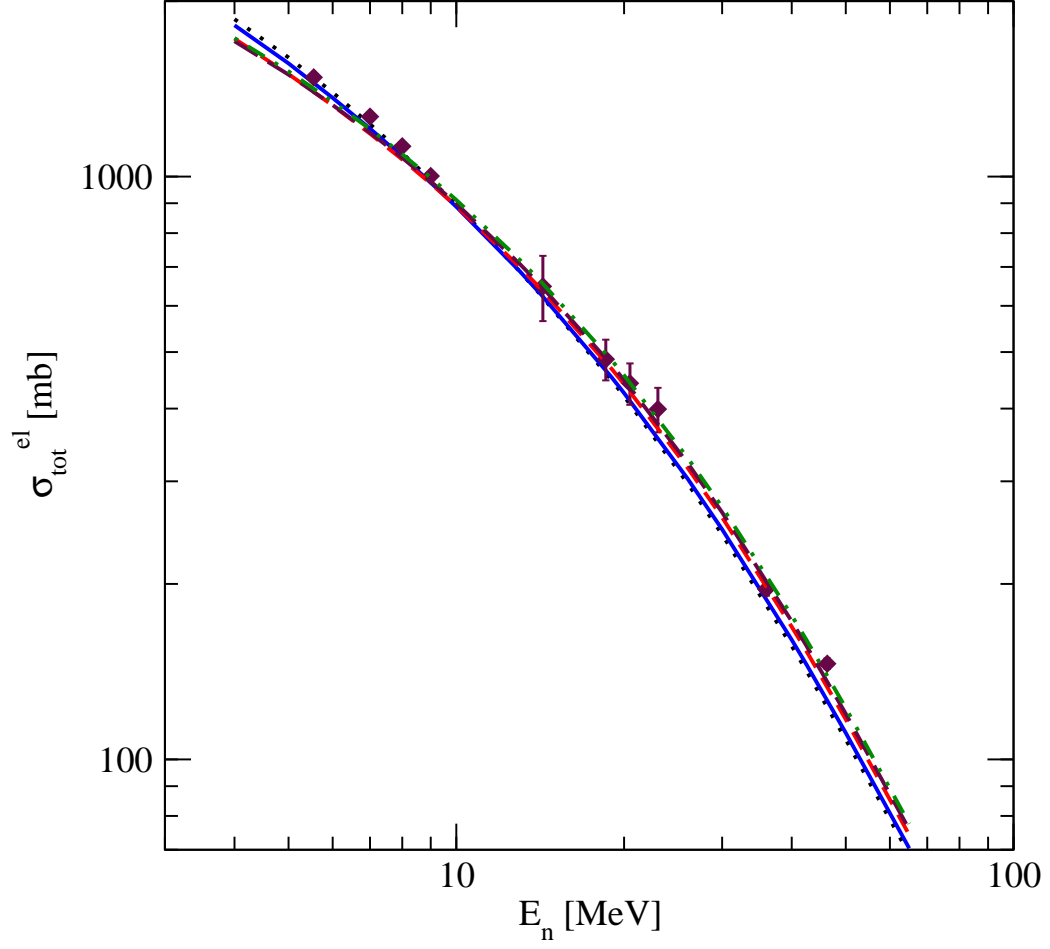


FIG. 2: (color online) The total neutron-deuteron elastic scattering cross section as a function of the neutron lab. energy. Different lines show sensitivity of that cross section to the changes of the  $nn\ ^1S_0$  force component. For their description see Fig.1. The (maroon) diamonds are nd data of Ref. [12].

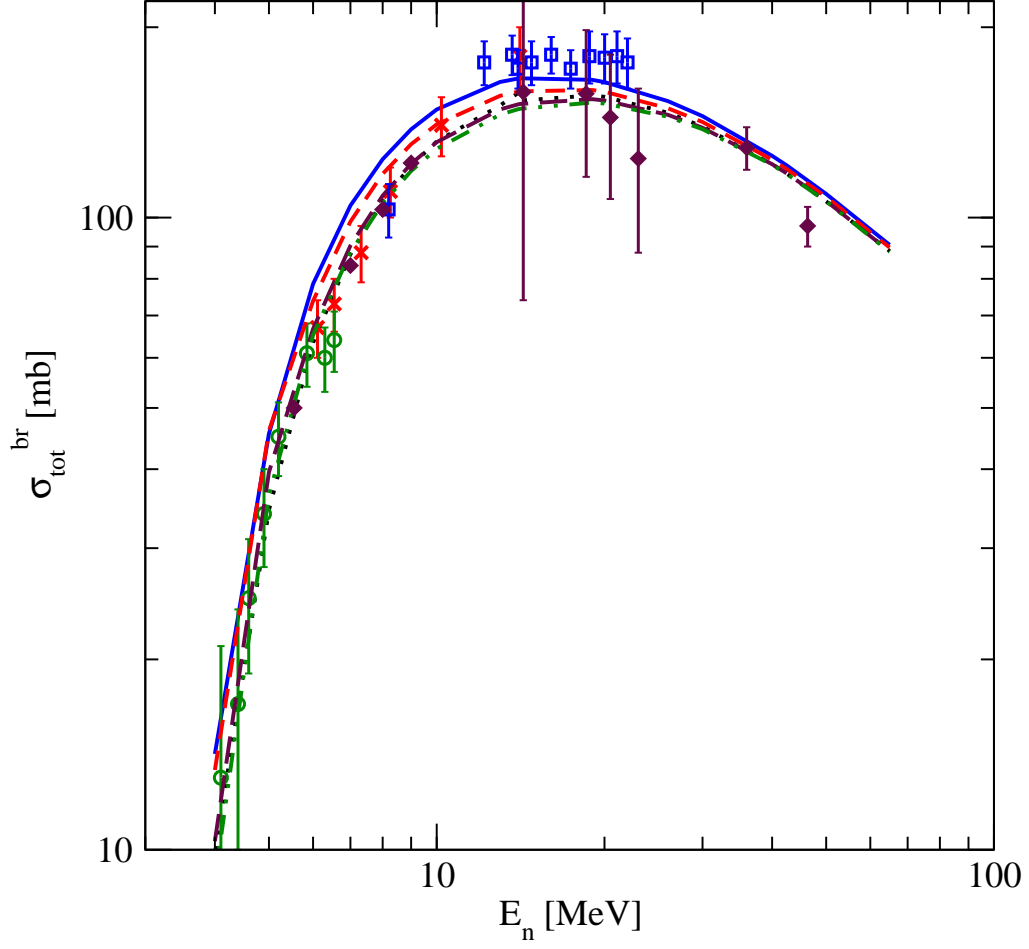


FIG. 3: (color online) The total neutron-deuteron breakup cross section as a function of the neutron lab. energy. Different lines show sensitivity of that cross section to the changes of the  $nn\ ^1S_0$  force component. For their description see Fig.1. The (red) crosses, (green) circles, (blue) squares, and (maroon) diamonds are nd data of Ref. [13], [14], [15] and [12], respectively.

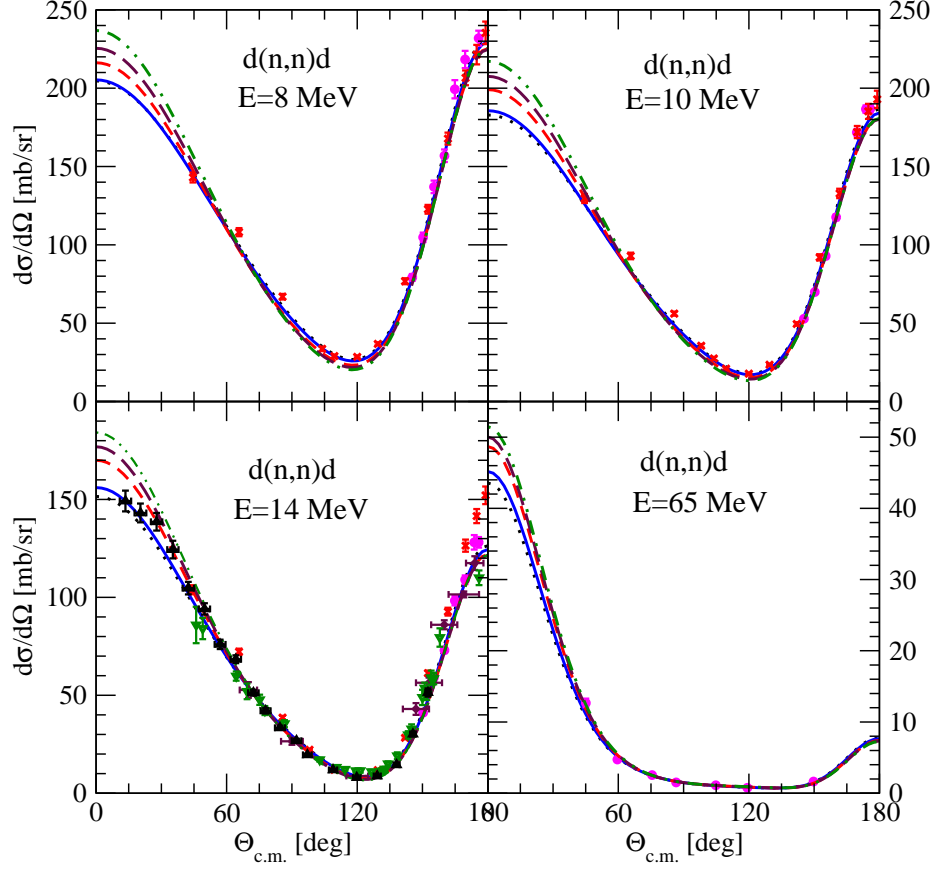


FIG. 4: (color online) The neutron-deuteron elastic scattering angular distributions  $d\sigma/d\Omega$  at a number of incoming neutron lab. energies. Different lines show sensitivity to the changes of the  $nn\ ^1S_0$  force component. For their description see Fig.1. At  $E_n = 8, 10$  and  $14$  MeV the (magenta) circles and (red) x-es are nd data of Ref. [18] and [11], respectively. At  $E_n = 14$  MeV the (maroon) stars, (green) triangle-down, and (black) triangle-up are nd data of Ref. [12], [19], and [20], respectively. At  $E_n = 65$  MeV the (blue) circles are  $E_n = 66$  MeV nd data of Ref. [21].

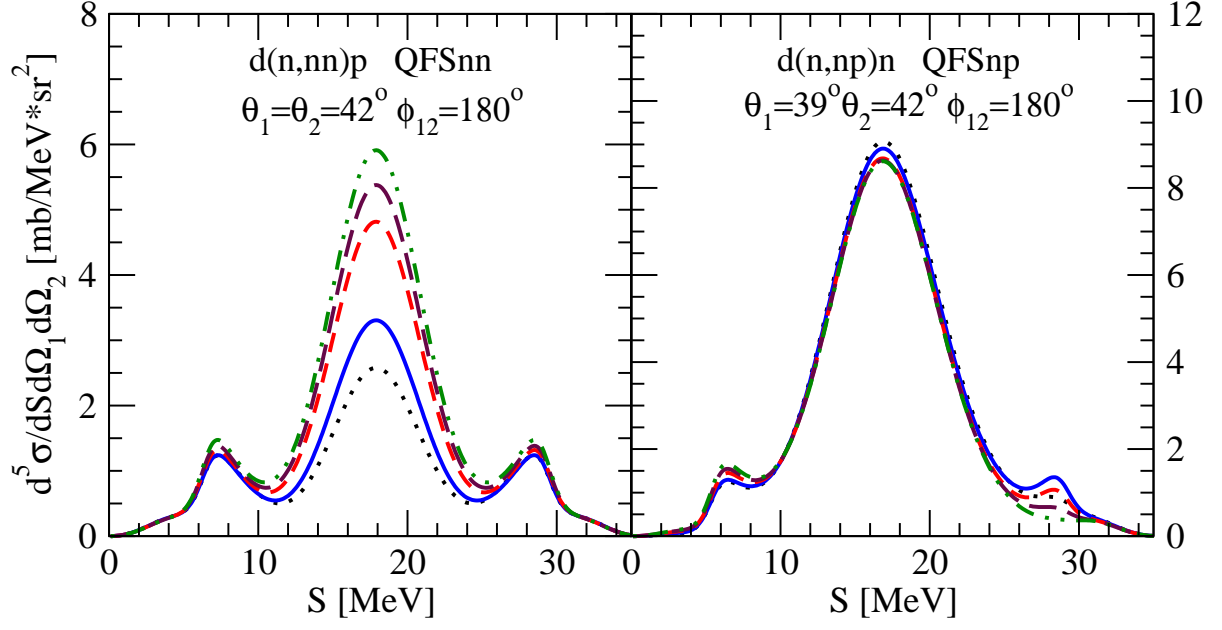


FIG. 5: (color online) The cross section  $d^5\sigma/d\Omega_1d\Omega_2dS$  as a function of the S-curve arc-length in the  $E_n^{lab} = 26$  MeV nd breakup reaction  $d(n,nn)p$  for the QFS nn (left) and np (right) kinematically complete configurations of Ref. [22]. For description of lines see Fig. 1.

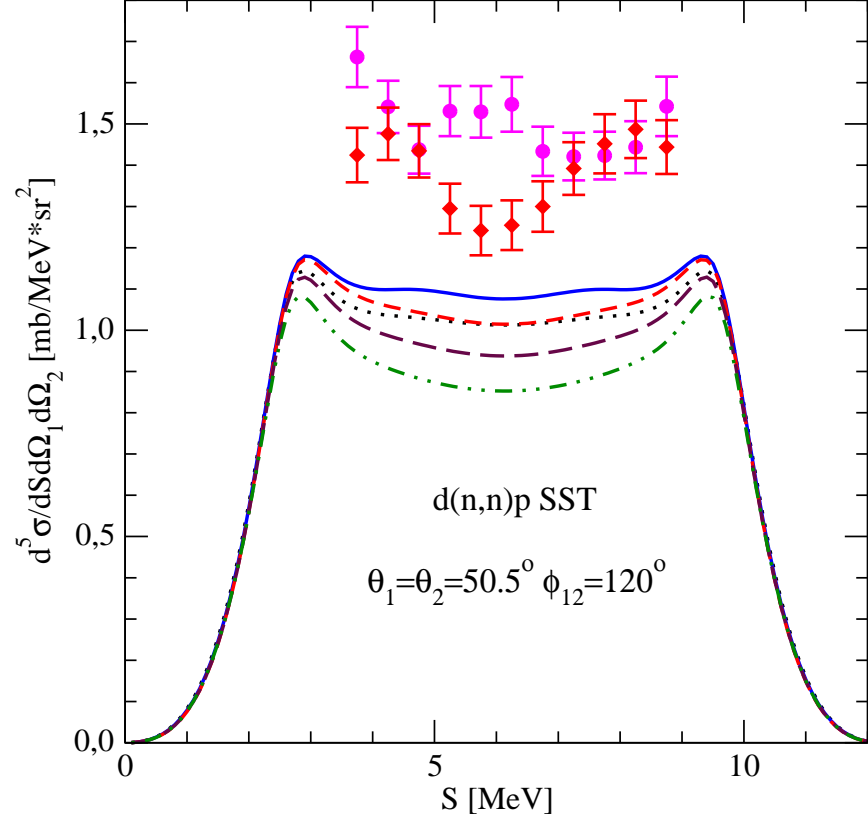


FIG. 6: (color online) The cross section  $d^5\sigma/d\Omega_1 d\Omega_2 dS$  as a function of the S-curve arc-length in the  $E_n^{lab} = 13$  MeV nd breakup reaction  $d(n,nn)p$  for SST configuration with the lab. angles of two detected neutrons  $\theta_1 = \theta_2 = 52.8^\circ$  and  $\phi_{12} = 180^\circ$ . For description of lines see Fig. 1. The (magenta) solid dots and (red) x-ses are nd data of Ref. [23, 24] and [25], respectively.

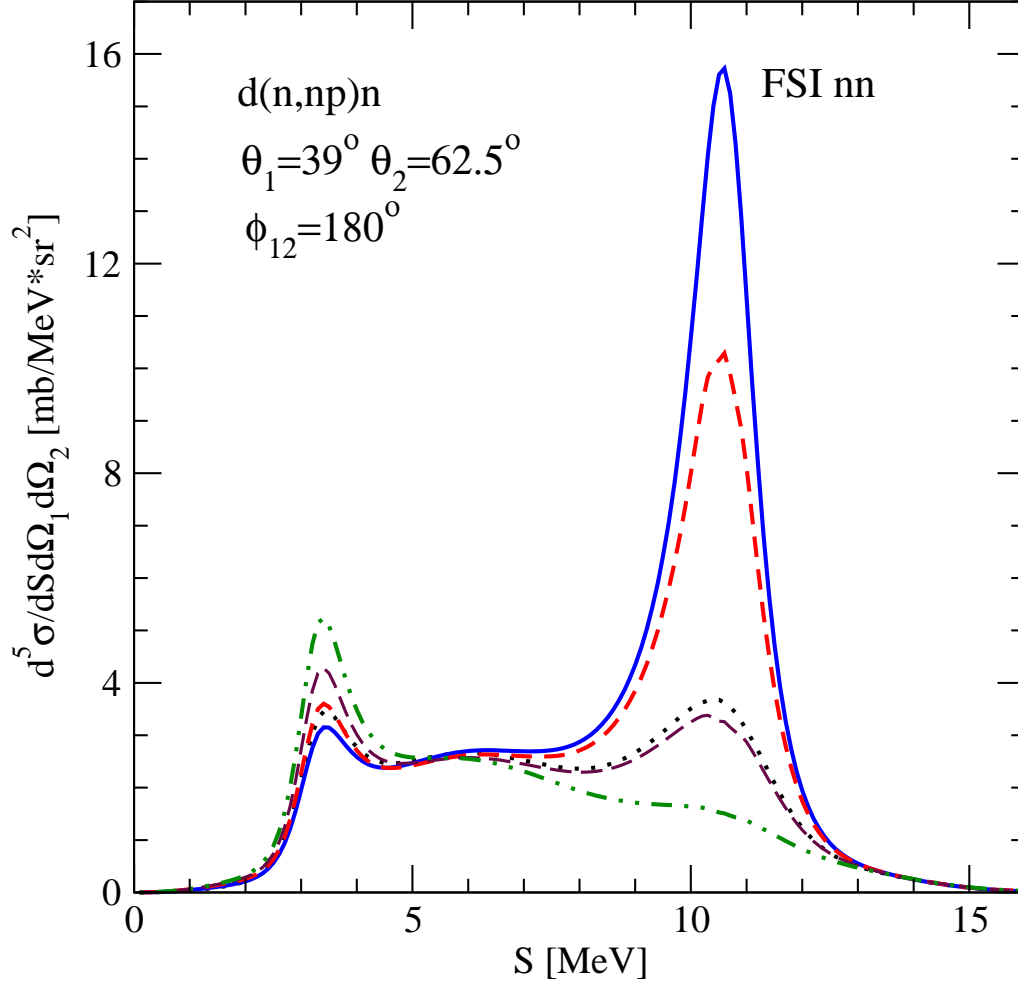


FIG. 7: (color online) The cross section  $d^5\sigma/d\Omega_1 d\Omega_2 dS$  for the  $E_n^{lab} = 13$  MeV nd breakup reaction  $d(n, np)n$  as a function of the S-curve length for nn FSI configuration. For description of lines see Fig. 1.

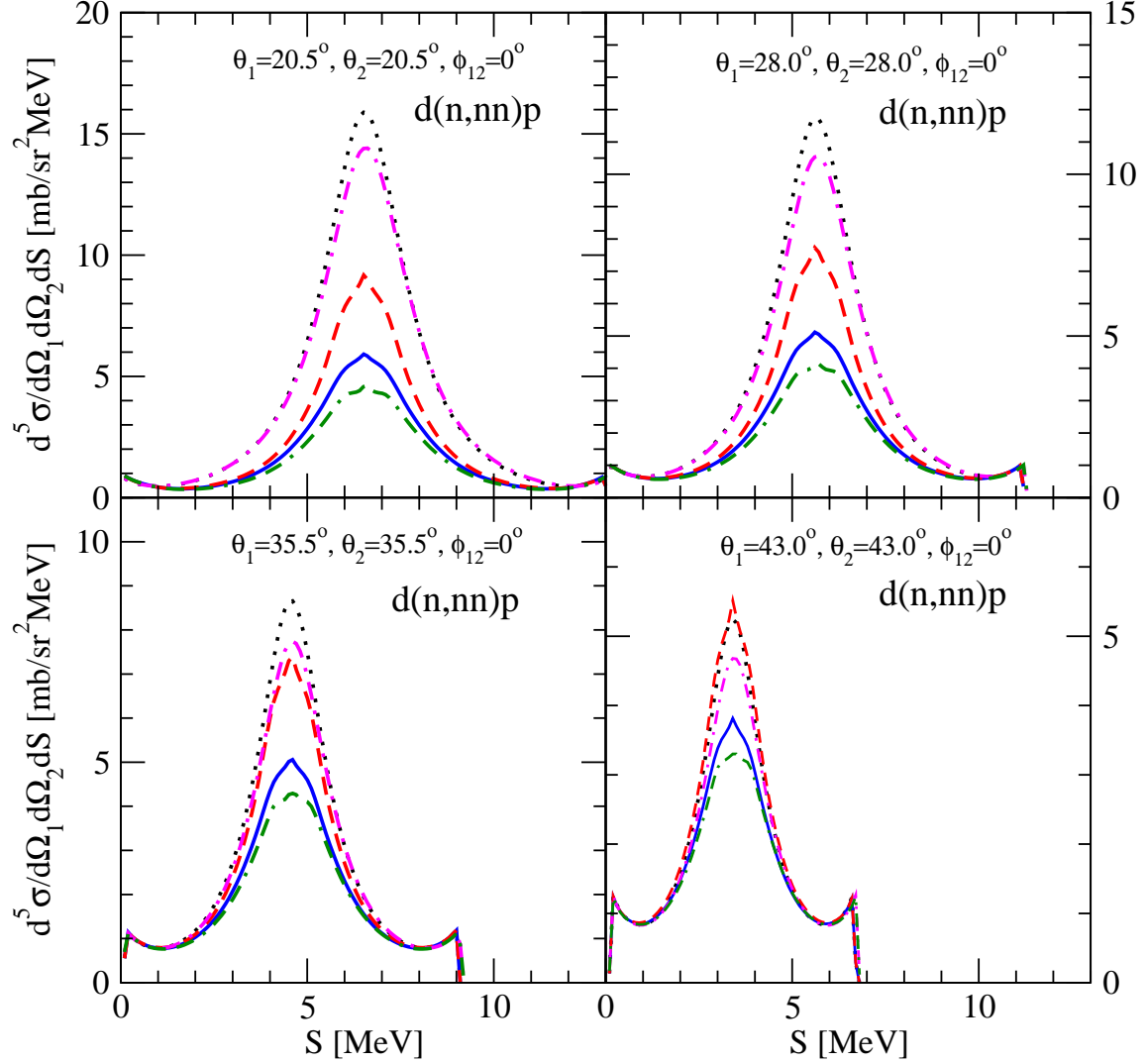


FIG. 8: (color online) The cross section  $d^5\sigma/d\Omega_1 d\Omega_2 dS$  as a function of the S-curve arc-length in the  $E_n^{lab} = 13$  MeV nd breakup reaction  $d(n,nn)p$  for 4 FSI nn geometries. Different lines show sensitivity of the cross section to the changes of the nn  $^1S_0$  force component. Those changes were induced for the dotted (black), (red) dashed and (blue) solid lines by multiplying the  $^1S_0$  nn matrix element of the CD Bonn potential by a factor  $\lambda$ . The dotted (black) line is the full result based on the original CD Bonn potential ( $\lambda = 1.0$ ) and all partial waves with 2N total angular momenta up to  $j_{max} = 3$  included. The (red) dashed and (blue) solid lines correspond to  $\lambda = 1.19$  and  $1.21$ , respectively. The (magenta) dashed-dotted and (green) double-dashed-dotted lines show results of Faddeev calculations based on NLO chiral perturbation theory potential and all partial waves with 2N total angular momenta up to  $j_{max} = 3$  included. They differ in the nn  $^1S_0$  force which for the (magenta) dashed-dotted line was obtained with the constants  $C_1(^1S_0) = 1.0$  and  $C_2(^1S_0) = 1.0$  (original NLO potential, see text for explanation) leading to  $a_{nn} = -17.6$  fm and  $r_{eff} = 2.75$  fm. For the (green) double-dashed-dotted line the constants  $C_1(^1S_0) = 1.50$  and  $C_2(^1S_0) = 1.29415$ , what results in  $a_{nn} = +17.5$  fm and  $r_{eff} = 2.41$  fm.



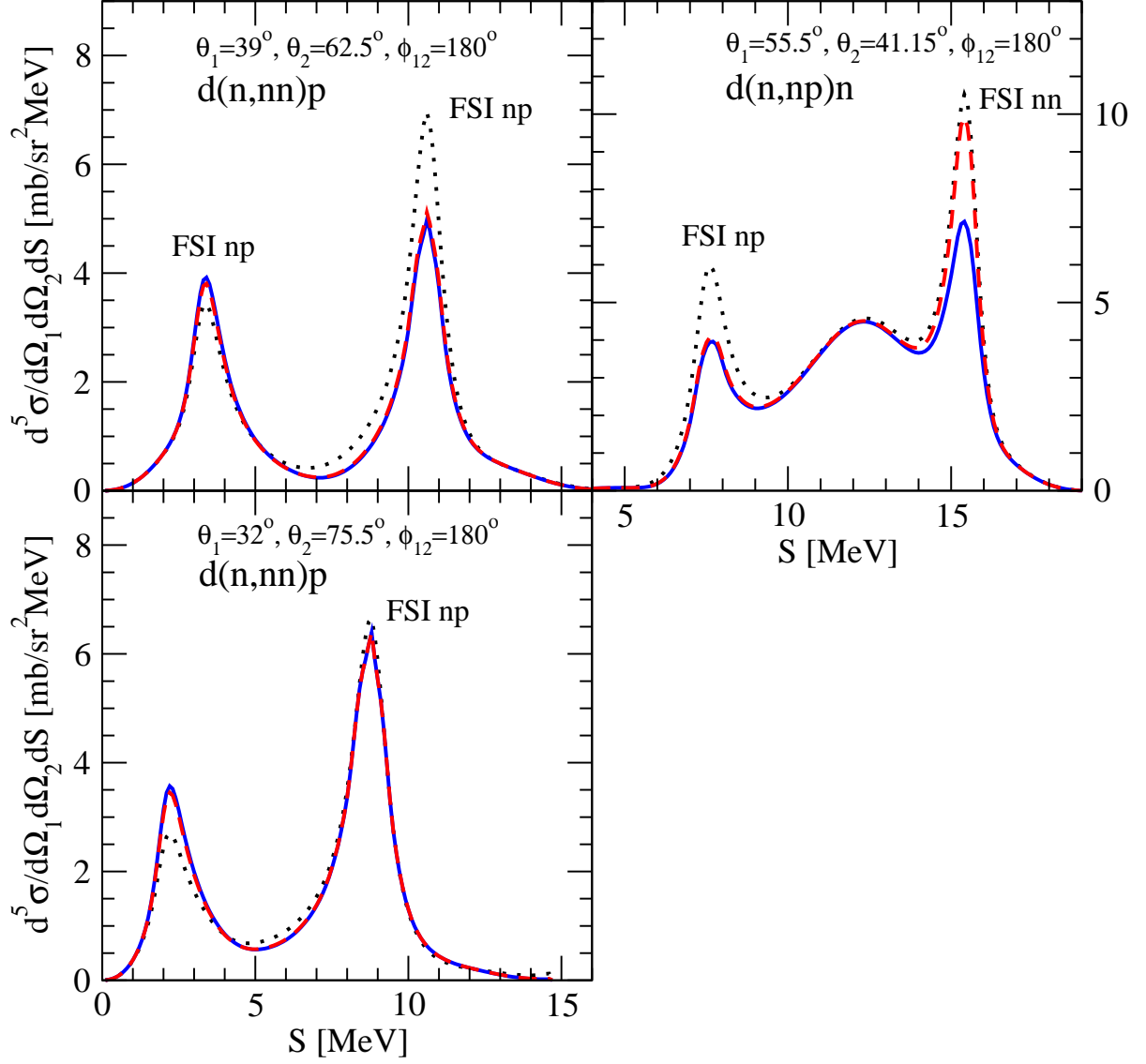


FIG. 9: (color online) The cross section  $d^5\sigma/d\Omega_1 d\Omega_2 dS$  as a function of the S-curve arc-length in the  $E_n^{lab} = 13$  MeV nd breakup reaction  $d(n,nn)p$  for 3 FSI geometries. Different lines show sensitivity of that cross section to the changes of the nn  $^1S_0$  force component. For their description see Fig.8.

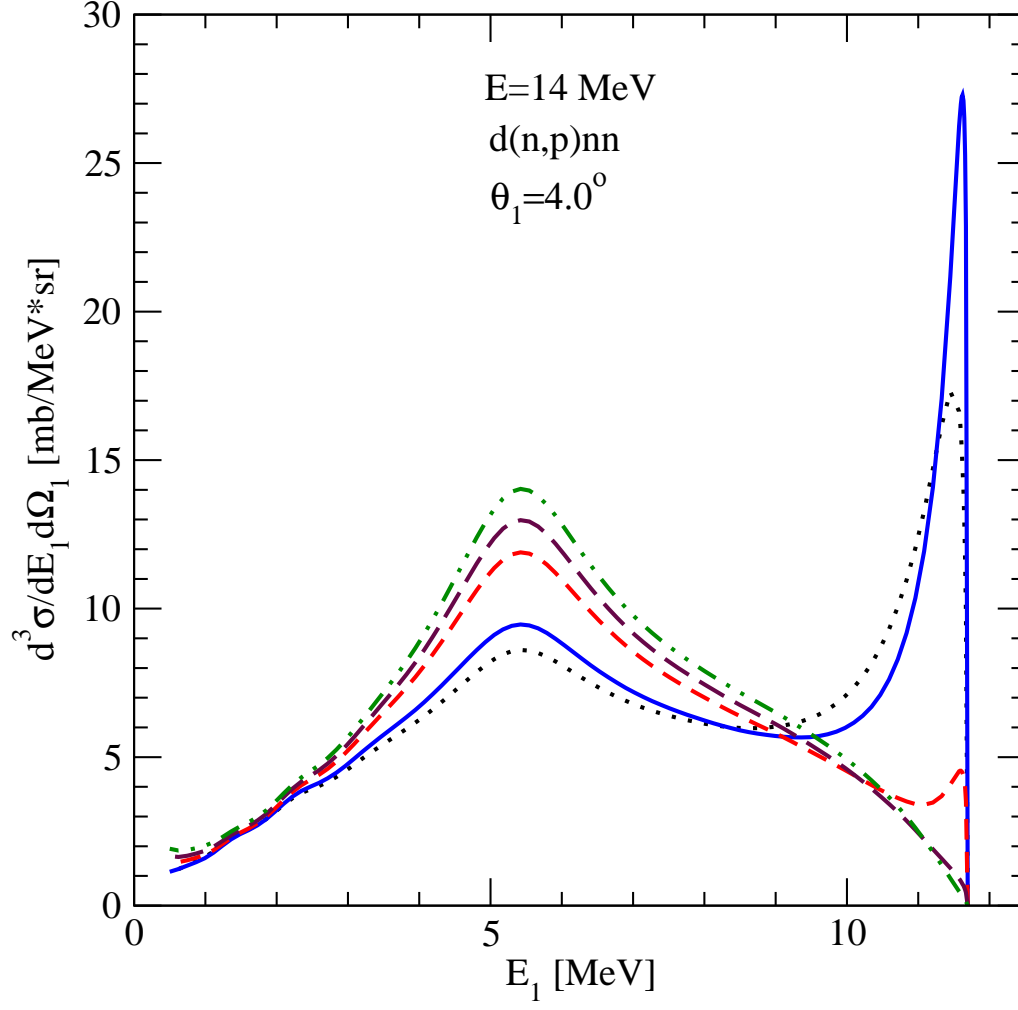


FIG. 10: (color online) The cross section  $d^3\sigma/d\Omega_1 dE_p$  for the  $E_n^{lab} = 14 \text{ MeV}$  uncomplete nd breakup reaction  $d(n,p)nn$  as a function of the outgoing proton lab. energy at the proton lab. angle  $\theta_1 = 4^\circ$ . For description of lines see Fig. 1.

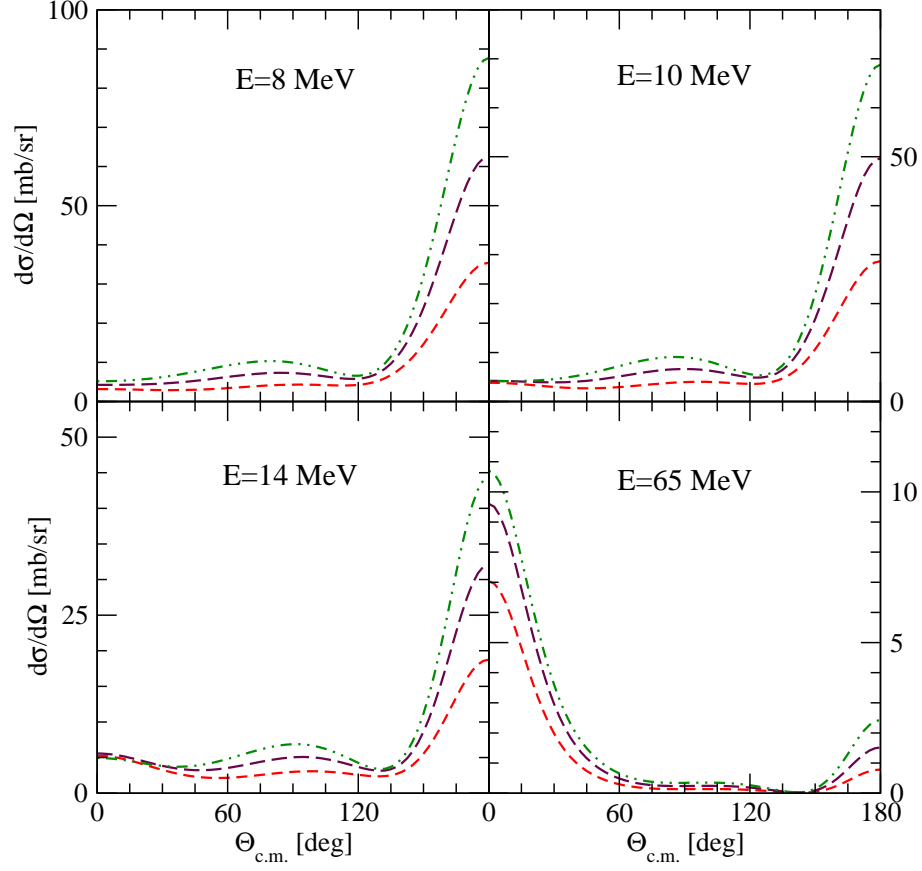


FIG. 11: (color online) The angular distributions  $d\sigma/d\Omega$  for  $d(n,p)d$ ineutron reaction at a number of incoming neutron lab. energies. The (red) short-dashed, (maroon) long-dashed, and (green) dashed-double-dotted lines correspond to the factor  $\lambda = 1.21, 1.3$ , and  $1.4$ , respectively.